

1
2
3
4
5
6
7
8
9
10
11
12
13
14
15
16
17
18
19
20
21
22
23
24
25
26
27
28
29
30
31
32
33
34
35

Technical Note:

Spectral slopes in deep, weakly-stratified ocean and coupling between sub-mesoscale motions and small-scale mechanisms

by Hans van Haren

Royal Netherlands Institute for Sea Research (NIOZ), P.O. Box 59, 1790 AB Den Burg,
the Netherlands.

e-mail: hans.van.haren@nioz.nl

36 Short summary. Large ocean circulations include small-scale physical processes like transport
37 by sub-mesoscale eddies and turbulence by internal wave breaking. Knowledge is lacking on
38 precise interaction between different processes. In deep weakly stratified waters, continuous
39 spectral slopes are observed that extend from sub-mesoscales across the internal wave band to
40 turbulence range. Such cross-spectral correspondence is suggested a potential feedback
41 mechanism stabilizing large-scale ocean circulations.

42

43 **Abstract.** Large, basin-wide ocean circulations are complex nonlinear dynamical systems.
44 They include small-scale physical processes such as, for example, transport by sub-mesoscale
45 eddies and turbulence-generating breaking of internal waves. To date however, knowledge is
46 lacking on precise interaction between different processes. In this note, a potential contributor
47 to interaction is investigated using spectra from deep-sea moored observations. In weakly
48 stratified waters, continuous spectral slopes are observed that extend from sub-mesoscales
49 across the internal wave band to turbulence range. In the latter, the governing slope can be
50 distinctly different from the inertial subrange of shear turbulence and is described as the
51 buoyancy subrange of convection turbulence. At sub-inertial frequencies, the slope's
52 extension either describes quasi-gyrosopic waves or sub-mesoscale eddies. Such cross-
53 spectral correspondence is suggested a potential feedback mechanism stabilizing large-scale
54 ocean circulations.

55

56 **1 Introduction**

57 The extent of anthropogenic influence on the Earth's climate warrants studies of the
58 ocean as a major player. Large, basin-wide ocean circulations are important for transporting
59 properties like heat, carbon and nutrients. Schematically, the Atlantic(-Ocean) Meridional
60 Overturning Circulation (AMOC) is depicted to transport heat from the equator to the poles
61 near the surface and carbon in the abyssal return (e.g., Aldama-Campino et al., 2023). It
62 includes physical processes like 'deep dense-water formation' in the polar region. Recent
63 mathematical and numerical modelling such as based on varying single parameters like sea-

64 surface temperature (e.g., Ditlevsen and Ditlevsen, 2023) and freshwater influx (e.g., van
65 Westen et al., 2024) suggest a potential future collapse of the AMOC. It is argued that this
66 may have consequences for Northwest-European climate.

67 Whilst the modelling might be robust mathematically, it lacks physical processes of
68 the drivers of the AMOC and observational evidence thereof. This will have consequences for
69 the feedback mechanisms at work in the nonlinear dynamical system of ocean circulation. As
70 has been reviewed for AMOC numerical models (Gent, 2018), important feedback
71 mechanisms are vertical turbulent mixing, sub-mesoscale gyre ‘eddy’ transport, and the
72 coupling with the atmosphere. Here we elaborate on the importance of turbulence induced by
73 internal wave breaking, possibly coupling with sub-mesoscale eddies (e.g., Chunchuzov et al.,
74 2021), and stability variations in vertical density stratification for such feedback, by
75 reviewing insights from recent modeling and deep-sea observations. In particular as an
76 example for complexity of dynamical system interactions, the core of ocean motions is
77 spectrally investigated focusing on most energetic mesoscale, internal wave, and turbulence
78 scales, for deep weakly stratified waters.

79 In contrast with the atmosphere, the ocean is not an effective heat engine (Wunsch
80 and Ferrari, 2004) despite its heat transportation. As a result, the AMOC is not predominantly
81 buoyancy-driven via push by deep dense-water formation near the poles (Marshall and Schott,
82 1999; Marotzke and Scott, 1999), which notably occurs in sporadic pulses rather than
83 continuously. Instead, the AMOC is mainly wind-steered (e.g., Liu et al., 2024) and tide-
84 driven, with turbulent mixing by internal wave breaking, and possibly associated upwelling
85 close to boundaries (Ferrari et al., 2016; McDougall and Ferrari, 2017), being considered an
86 important physics process of pull that dominates over push by a heat engine. Winds, near the
87 ocean surface, and tides, via interaction with seafloor topography deeper down, contribute
88 about equally to generate internal waves that are found everywhere in the ocean interior. Such
89 waves break predominantly at ubiquitous underwater seamounts and continental slopes.

90 Without turbulent mixing, the AMOC would be confined to a 100-m thick near-
91 surface layer and the deep-ocean would be a stagnant pool of cold water (Munk and Wunsch,

1998). This is not the case however, and the solar heat is mixed from the surface downward so that the ocean is stably stratified in density all the way into its deepest trenches, as has been shown in hydrographic deep-ocean observations (Taira et al., 2005; van Haren et al., 2021a). Although turbulent mixing by internal wave breaking in the ocean-interior is insufficient by at least a factor of two to maintain the vertical density stratification (e.g., Gregg, 1989, Polzin et al., 1997), such breaking along ocean boundaries has been suggested to be more than sufficient (Munk, 1966; Polzin et al., 1997). Especially large internal wave breaking is expected to occur above steeply sloping topography (Eriksen, 1982; Thorpe, 1987; Sarkar and Scotti, 2017). Because there are more and larger seamounts than mountains on land, equally abundant sloping seafloors lead to abundant turbulent mixing, as has been charted from recent observations and modelling results summarized below.

As recent observations (van Haren and Dijkstra, 2021; van Haren et al., 2024) demonstrate that breaking waves can lead to considerable buoyancy driven convection turbulence, this note attempts further understanding of a little studied deep-sea complex process and its potential interaction with sub-mesoscale motions. The sub-inertial range of sub-mesoscale motions has rarely been a subject of oceanographic spectral observations. Knowledge about such small-scale processes and their interactions may be vital for understanding potential feedback mechanisms affecting the stability of large-scale ocean circulations.

111

112 **2 Recent internal wave breaking results**

Detailed observations and numerical modeling have revealed the extent of internal tide breaking processes above ocean topography (van Haren and Gostiaux, 2012; Winters, 2015; Wynne-Cattanach et al., 2024). Using high-resolution observations (e.g., van Haren and Gostiaux, 2012), internal tide breaking above steep deep-sea slopes is observed to generate spring-neap-average turbulent vertical diffusivity value of about $3 \times 10^{-3} \text{ m}^2 \text{ s}^{-1}$. This value is twice the value theoretically required to yield upwelling in a thin layer above sloping topography (McDougall and Ferrari, 2017). Such quantification of turbulent mixing shows

120 that it occurs with typical tidal-period-average values that are more than 100 times larger over
121 super-critical slopes than open-ocean values. A super-critical seafloor slope is steeper than the
122 slope of internal wave characteristics. While ocean-wide tides energetically dominate internal
123 waves, not all seafloor slopes are super-critical for these waves. In contrast, nearly all seafloor
124 slopes are super-critical for at least one component of secondary energetic near-inertial
125 waves, which are generated via geostrophic adjustment following the passage or collapse of a
126 disturbance such as fronts or atmospheric storms on the rotating Earth. Under common
127 stratification, near-inertial waves are at the lowest frequency of freely propagating internal
128 waves. The highest frequency propagating internal waves, near the buoyancy frequency,
129 experience nearly vertical walls as super-critical seafloor slopes.

130 Within a tidal, or near-inertial, period, turbulence peaks in bursts of shorter duration
131 than half an hour when highly nonlinear internal waves propagate as internal bores up a
132 super-critical slope, once or twice a tidal cycle. The breaking of bores leads primarily to
133 convection, buoyancy-driven turbulence, rather than frictional shear-turbulence over the
134 sloping seafloor and occur at a wide variety of deep-sea and deep-ocean locations (e.g., van
135 Haren et al., 2013; van Haren et al., 2024). Between bores, the turbulent mixing varies by an
136 order of magnitude in intensity, with effects extending about 100 m vertically and several
137 kilometers horizontally from the seafloor. Although intermittently occurring at a given
138 position of the sloping seafloor and about 10% varying in arrival time, the turbulence is
139 generated internally by the tide, for about 60% (Wunsch and Ferrari, 2004), and by winds, for
140 about 40%, in a stratified ocean-environment. The turbulent bores also resuspend sediment
141 and thereby replenish nutrients away from the seafloor (Hosegood et al., 2004), important for
142 deep-sea life. Enhanced turbulent mixing above sloping boundaries has a demonstrated effect
143 on the outcome of general ocean circulation models (e.g., Scott and Marotzke, 2002), with
144 predicted subtle effects on upwelling near the seafloor (Ferrari et al., 2016).

145 The complexity of turbulence generation, mixing and restratification, are still subjects
146 of deep-ocean research. While shear-induced turbulence has been relatively well studied in
147 the stratified ocean, deviations such as convection-turbulence are little observed, with recent

148 exceptions (van Haren and Dijkstra, 2021; van Haren et al., 2024). Convection turbulence is
149 dominant in the atmosphere especially during daytime, and has also been observed in the
150 near-surface ocean during nighttime (e.g., Brainerd and Gregg, 1995), but it has never been
151 quantitatively directly observed in deep dense-water formation zones (Thorpe, 2005) and
152 above geothermal vents.

153 Deep dense-water formation does not only occur in polar seas, but occasionally also
154 in the at least 10°C warmer Mediterranean (Gascard, 1978), with an important contribution of
155 atmospheric exchange due to orographic generated winds affecting the preconditioning by
156 cooling and drying of near-surface waters. Similarly, internal waves occur in oceans and in
157 the Mediterranean under stratification conditions that vary over at least one order of
158 magnitude in time and space, but tides are relatively weak in the Mediterranean, and yet
159 ‘sufficient’ turbulent diapycnal mixing, sufficient for maintenance of deep-sea stratification
160 and thereby driving overturning circulation, is generated via the breaking above topography
161 of near-inertial motions mainly (van Haren et al., 2013). Further complications are expected
162 from interactions of internal waves with sub-mesoscale eddies and potential consequences of
163 varying intensity thereof, e.g., on seasonal scales.

164

165 **3 Mediterranean observations as an example proxy for ocean conditions**

166 In many physical oceanographic aspects of heat and salt budgets, large-scale water-
167 flow circulation, strong boundary flow, eddies at sub-mesoscales, near-inertial motions
168 including gyroscopic waves and internal wave turbulence, the Mediterranean Sea can be
169 considered a sample for the state of the much larger oceans (e.g., Gascard, 1973; Crepon et
170 al., 1982; Garrett, 1994; Millot, 1999; van Haren and Millot, 2004; Testor and Gascard,
171 2006). Like in oceans, the Mediterranean seafloor reaches great depths and can be rugged
172 with steep slopes in places, including continental slopes incised by deep canyons.

173 In the Northwest Mediterranean, vertical density stratification varies markedly with
174 seasons and years, having relatively large near-surface values in summer and relatively low
175 values in winter. The proximity of extensive mountain ranges on land generates highly

176 variable winds that can cool and dry surface waters. In winter in weaker stratified waters, this
177 may lead to unstable conditions of buoyancy driven convection in an exchange of dense-water
178 sinking down, and less dense-waters up. Like in the polar regions, such exchange can be
179 observed daily in the upper 10 m from the sea-surface, regularly down to a few 100 m from
180 the surface, and seldom, once every 5-8 years (e.g., Rhein, 1995; Mertens and Schott, 1998),
181 down to the abyssal seafloor at about 2500 m. In contrast, horizontal density gradients
182 associate with forcing of a dynamically unstable boundary current and eddies at multiple 1-
183 100 km sub-mesoscales (e.g., Crepon et al., 1982; Testor and Gascard, 2006). These eddy
184 motions may push relatively warm waters down, thereby increasing the weak stratification in
185 the deep-sea.

186 In summer, atmospheric disturbances are less intense, near-surface stratification is
187 large due to solar heating, and eddy activity associated with some continental boundary flows
188 is weaker (Alb rola et al., 1995). This opens the possibility for detection of near-inertial wave
189 dominance in kinetic energy. In relatively strong stratification, mainly gravity-driven parts of
190 near-inertial waves generate largest vertical current differences ‘shear’ that destabilize
191 stratification due to their relatively short vertical length-scale, not only in the Mediterranean
192 but also as observed in the Atlantic Ocean (van Haren, 2007). This destabilization may lead to
193 small-10-m vertical scale layering of near-homogeneous waters throughout seas and oceans.
194 On larger-100-m vertical scales near-homogeneous waters occur in deep waters of the
195 Mediterranean as well as of North-Atlantic basins like the Bay of Biscay and Canary Basin.
196 In near-homogeneous water-layers with weak stratification, gyroscopic, Earth-rotation-driven,
197 parts of near-inertial waves dominate and result in 0.1-1 km diameter smaller than sub-
198 mesocale tubes of slantwise rather than vertical convection (Emanuel, 1994; Marshall and
199 Schott, 1999; van Haren and Millot, 2004). Hence, one may expect frequency spectra of non-
200 tidal dominated data from instruments moored in the Mediterranean reveal convection and
201 thus deep transport under winter and summer conditions.

202 It is noted that ocean-spectra may show peaks such as at narrowband tidal and at,
203 broader band, inertial frequencies, but they lack gaps. This lack of spectral gaps potentially

204 couples motions at sub-inertial with inertial-buoyancy internal wave with super-buoyancy
205 turbulence frequency ranges. However, it is unclear how such a coupling may work as some
206 motions represent two-dimensional ‘2D’ eddies, some linear waves, some non-linear waves,
207 some anisotropic stratified turbulence, and some isotropic 3D turbulence. This is investigated
208 by renewed spectral analysis below, using, in analogy, slopes typical for investigating energy
209 cascades in turbulence research.

210

211 **4 Uncommon slopes in revisited spectra**

212 Kinetic energy (KE) spectra from historic moored current meter observations down to
213 mid-depth $z = -1100$ m in the Ligurian Sea under upper-sea strongly stratified ‘summer’ and
214 weakly stratified ‘winter’ conditions surely lack gaps (Fig. 1). Year-round at $z = -1100$ m, the
215 buoyancy frequency N , reflecting the square-root of vertical density stratification, is small N
216 $\sim O(f)$, f denoting the inertial frequency involving Earth rotation. This narrows the local
217 internal wave band, while, especially in winter, sub-mesoscale activity is large in the area,
218 and, occasionally, the few moored current meter temperature records showed inversions (van
219 Haren and Millot, 2003). Although these hourly sampled data barely resolve the turbulence
220 ranges at frequencies $\omega > N$, the internal wave continuum was suggested to scale like ω^p ,
221 with, on a log-log plot, ‘spectral slope’ $p = -2.2 \pm 0.4$, independent of location and season
222 albeit with different KE (power) levels.

223 Within the uncertainty range, several possible explanations can be given for the
224 observed spectral slope. Freely propagating internal gravity waves have been fitted to $p = -$
225 2 ± 0.5 but only for $f \ll \omega \ll N$ (Garrett and Munk, 1972). Considering that the data in Fig. 1
226 are from a site where locally $N = (3 \pm 2)f$, irrespective of season (van Haren and Millot, 2003),
227 alternative explanations were sought for observed spectral slopes at sub-inertial frequencies
228 $0.2 \text{ cpd} < \omega < f$. Cpd is short for ‘cycles per day’. An obvious candidate is ‘fine-structure
229 contamination’ of step functions passing sensors, which gives a theoretical value of $p = -2$
230 (Phillips, 1971; Reid, 1971). For their winter data, van Haren and Millot (2003) attributed

231 such a slope to evidence intense mesoscale activity, because of the continuation of slope up to
232 $\omega = 5$ cpd before rolling off near the Nyquist frequency. However, they did not elaborate.
233 Below, the data in Fig. 1 are re-analyzed from the perspective of convection-turbulence.

234 Theoretical considerations of non-zero-mean flow convection-turbulence suggest a
235 spectral scaling in the buoyancy subrange having $p = -11/5 = -2.2$ for KE, and $p = -7/5$ for an
236 active scalar quantity. This ‘BO’-scaling follows atmospheric and theoretical works by
237 Bolgiano (1959) and Obukhov (1959). The scaling was set-up for a stably stratified
238 atmospheric environment for the anisotropic part in which turbulent kinetic energy is partially
239 transferred to potential energy leading to turbulent convection. Later works extended BO-
240 scaling to purely buoyancy-driven turbulence, e.g., for Rayleigh-Bénard convection (Lohse
241 and Xia, 2010) and Rayleigh-Taylor instabilities (Poujade, 2006; Celani et al., 2006).

242 Laboratory experiments on such gravitationally driven convection are inconclusive on
243 BO-scaling. On the one hand, this scaling is confirmed for both KE and temperature in
244 experiments by Ashkenazi and Steinberg (1999), while on the other hand it is only confirmed
245 for scalars by Pawar and Arakeri (2016) who found a slope of $p = -5/3$ for KE. The $p = -5/3$ -
246 slope suggests dominance of shear-induced turbulence of the inertial subrange for equilibrium
247 isotropic turbulence cascade in the ‘KO’-scaling (Kolmogorov, 1941; Obukhov, 1949) but
248 should also be found in spectra of scalars that are passive in this range. While Liot et al.
249 (2016) show KO-scaling in their model that may have to do with their Lagrangian data as
250 proper transfer brings the data closer to BO-scaling, Poujade (2006) and Cenari et al. (2006)
251 show clear BO-scaling in their models. This suggests particular conditions do affect the
252 dominance of shear- or convection-turbulence. It is noted that BO-scaling is also simply
253 considered as a significant deviation from KO-scaling, which is more commonly observed in
254 stratified shear flows.

255 Obviously, scalars cannot be passive and active at the same time and in the same
256 space. This discrepancy between types of scaling between scalars and KE may be because the
257 laboratory experiments of Pawar and Arakeri (2016) were in zero mean flow. Also, under
258 sufficiently stable conditions without shear, no inertial subrange is expected (Bolgiano, 1959).

259 However, the spectral extent of BO-scaling is largely unknown albeit it is more generally
 260 found adjacent to higher-frequency inertial subrange. While KO-scaling is based on a forward
 261 cascade of energy, the direction of energy cascade is inconclusive for BO-scaling and may be
 262 partially forward and partially backward, at least as reasoned for pure buoyancy-driven
 263 convection-turbulence (Lohse and Xia, 2010). Probably, directions of cascade change with
 264 locality in the flow, and perhaps depend on scale, which would also imply that KO- and BO-
 265 scaling cannot be found at the same site.

266 Revisiting data from non-zero mean flow and weakly stratified deep-sea in Fig. 1
 267 demonstrates the possibility of fit of $p = -11/5$ outside near-inertial harmonic peaks. In winter,
 268 such a fit is observed consistently through the entire range of $0.2 < \omega < 5$ cpd. In traditional
 269 terms, this frequency range covers the transition from mesoscale $\omega < f$, via internal wave $f <$
 270 $\omega < N$, to turbulence $\omega > N$ motions. In summer, the $p = -11/5$ -slope is found at two different
 271 KE levels for bands $0.2 < \omega < \omega_{\min}$ and $2\Omega < \omega < 5$ cpd at sub- and super-IGW frequencies,
 272 respectively. Here, $\omega_{\min} \leq f$ denotes the minimum frequency bound for inertio-gravity waves
 273 IGW (LeBlond and Mysak, 1978), and Ω the Earth rotational frequency. Maximum IGW
 274 frequency is denoted by $\omega_{\max} \geq 2\Omega$, N . The ω_{\min} and ω_{\max} are functions of N , latitude φ and
 275 direction of wave propagation (LeBlond and Mysak, 1978; Gerkema et al., 2008),

$$276 \quad \omega_{\max}, \omega_{\min} = (A \pm (A^2 - B^2)^{1/2})^{1/2} / \sqrt{2}, \quad (1)$$

277 in which $A = N^2 + f^2 + f_s^2$, $B = 2fN$, and $f_s = f_h \sin \alpha$, α the angle to φ . For $f_s = 0$ or $N \gg 2\Omega$,
 278 the traditional bounds $[f, N]$ are retrieved from (1). The plotted IGW-bounds $[\omega_{\min}, \omega_{\max}]$ are
 279 for weakly stratified, near-homogeneous layers in which $N = f$. This weak stratification would
 280 lead to an impossible wave solution under the traditional approximation, but (1) allows wave
 281 propagation, albeit horizontally for one component (e.g., Gerkema et al., 2008).

282 The bridge between the KE-levels at sub- and super-IGW is formed by the finitely
 283 broad near-inertial peak. The base of this peak is proposed to slope like $p = -1$ reaching super-
 284 IGW BO-scaling at about $\omega \approx 4$ cpd $\approx N$. Such $p = -1$ -slope has been observed for the KE-
 285 spectral continuum between $[f, N]$ from the deep Bay of Biscay, Northeast Atlantic Ocean

286 (van Haren et al., 2002). Theoretically, this slope represents spectral scaling of intermittency
287 of a weakly chaotic nonlinear system (Schuster, 1984), i.e., 3D dynamical systems that evolve
288 into self-organized critical structures of states which are minimally stable (Bak et al., 1987).
289 Such a spectral bridge, or hump, is expected for turbulence in unstable stratification, as has
290 been illustrated using atmospheric observations (Lin, 1969). It is attributed to the flow field
291 absorbing energy from the scalar temperature field as potential energy is transferred to kinetic
292 energy. It is not clear to what extent near-inertial internal waves contribute in a similar way to
293 spectral redistribution of energy in our oceanographic data. As the observations from the
294 central Ligurian Sea show similar results, the hump is unlikely associated with seafloor slopes
295 matching the slope of near-inertial internal wave rays.

296 These spectral observations suggest a dominance of convection cascade from sub-
297 meso- via IGW- to, probably because unresolved, turbulence-scales under high-energetic
298 winter-conditions as they show a continuous slope across their frequency ranges. Such a
299 cascade is also suggested under quieter summer conditions when, however, it is masked by
300 IGW that lead a cascade at $\omega > \omega_{\min}$. Especially the sub-inertial range of apparent BO-scaling
301 seems out of the turbulence range, unless waters are near-homogeneous $N \rightarrow 0$ so that $\omega_{\min} \rightarrow$
302 0, from (1). This would extend not only IGW, notably gyroscopic waves, but also turbulence,
303 probably in the form of slantwise convection, to the sub-mesoscale range.

304 For the mesoscale range, the observations in Fig. 1 are supported by numerical
305 modeling results that have suggested eddy-KE has a broad range of spectral slopes between -3
306 $< p < -5/3$ (Storer et al., 2022), and by satellite altimetry observations that indicated, after
307 noise-correction and transfer to KE, a best-fit of $p = -2.28$ (Xu and Fu, 2012). No mention
308 was made of BO-scaling, but the correspondence seems evident.

309 As the KE in Fig. 1 is at least one order of magnitude larger in winter than in
310 summer, a near-inertial peak, if it exists, will be part of the spectral continuum during the
311 former. The winter observations suggest a continuous spread of sub-mesoscale energy across
312 the IGW band including inertial motions and into the turbulence range. In winter, near-surface

313 stratification is considerably weaker than in summer, so that local atmospheric-generated
314 near-inertial motions will be smaller. It is noted that the signals near the Nyquist frequency
315 not only contain instrumental white noise, but also unresolved turbulence motions, which are
316 also larger in winter than in summer.

317 Inspired by Western Mediterranean observations, Saint-Guilly (1972) proposed from
318 theoretical work that winter-time inertial KE is spread over a broad featureless band, like
319 quasi-gyroscopic waves that may be present between IGW-bounds (1) for $N \sim f$ (LeBlond and
320 Mysak, 1978; Gerkema et al., 2008). However, observations from the year-round upper-layer-
321 stratified central Western Mediterranean demonstrate that, also in deep homogeneous $N = 0$
322 waters, a near-inertial peak can be observed in KE-spectra (van Haren and Millot, 2004). This
323 may be attributed to a year-round source of atmospheric-generated inertial waves that are the
324 only internal waves that can propagate without attenuation from well-stratified to near-
325 homogeneous layers and vice versa (van Haren, 2023b).

326 Based on limited spectral observations, Gascard (1973) suggested the generation of
327 12-h stability waves, close to the buoyancy frequency of very weak stratification, which may
328 briefly force dense-water formation, thereby implicitly suggesting a link between internal
329 waves and sub-mesoscale eddies. As such eddies have estimated relative vorticity of $|\zeta| = f/2$
330 in the Western Mediterranean (Testor and Gascard, 2006), this addition to the planetary
331 vorticity (f) automatically widens the ‘effective’ near-inertial band $0.5f < f_{\text{eff}} < 1.5f$, of which
332 the bounds are close to IGW-bounds for $N = 0.8f$. One of the properties can be a modification
333 of near-inertial frequency (Perkins, 1976), and trapping with downward propagation of near-
334 inertial waves in anticyclonic eddies (Kunze, 1985; Voet et al., 2024). Such frequency
335 modification may add to local physics of inertial wave caustics due to latitudinal variation
336 (LeBlond and Mysak, 1978), which however can only lead up to 15% change in f in the
337 Mediterranean. Although found to be limited to the rather flat KE-spectral dip in the
338 immediate half-order-of-magnitude sub-inertial frequency band, standing vortical modes, i.e.
339 low-frequency non-propagating motions, of vertical length-scale < 10 m are suggested to be as
340 energetic as internal waves (Polzin et al., 2003). Alternatively, it has been suggested for

341 North-Atlantic observations that vortical modes may interact with internal waves, affecting
342 internal-wave shear that was peaking over $O(10)$ m vertical scales at IGW-frequencies in a
343 band with limits determined by weak stratification as in $N = f$ (van Haren, 2007).

344 For hypothetical $\omega_{\min} = 0.2$ cpd, at which the observed spectral slope changes away
345 from $p = -11/5$ (Fig. 1), one would require $N = 0.21f$, which is almost unmeasurable and non-
346 existent for any prolonged period even in the deep Northwestern Mediterranean, to the
347 knowledge of the author. However, it may reflect ω_{\min} computed using $f_{\text{eff}} = 0.5f$ and $N = f_{\text{eff}}$,
348 noting that such conditions can only apply for part of the record. If so, it would reflect a direct
349 coupling between sub-mesoscale and IGW-motions with slantwise convection (Marshall and
350 Schott, 1999; van Haren and Millot, 2004; Gerkema et al., 2008). The $p = -11/5$ is
351 significantly distinguishable from -2 over a frequency range of nearly two orders of
352 magnitude, and from $-5/3$ over a range of just over half an order of magnitude (Fig. 1). The
353 roll-off to noise (slope 0), for $\omega > 5$ cpd, may partially be seen as following a slope of $p = -5/3$
354 before 0. The roll-off around 0.1 cpd suggests an unresolved broad mesoscale peak-value
355 between 0.01 and 0.1 cpd. While these 1980's moored current meter data barely resolved the
356 turbulence part of the KE-spectrum, and thus also not the $p=-5/3$ inertial subrange slope, their
357 temperature sensors were too poor to simultaneously verify any spectral scaling for scalars.

358 About 40 years later, high-resolution and high-precision moored temperature sensor
359 'T-' data provided opportunity to verify scalar spectral scaling of turbulence energetic
360 motions in the area. These T-data evidenced occasional warming of the deep Northwest
361 Mediterranean seafloor (Fig. 2a), which, after comparison with data from higher-up appeared
362 to be coming from above, or slanted sideways, under relatively stratified conditions, and from
363 general non-vents geothermal heating from below (van Haren, 2023a). The data were
364 collected during mid-fall, when near-surface waters were well stratified and no cold, dense-
365 water production through convection was observed. Locally near the seafloor, the broad two-
366 day warming around day 308 is most stratified, whilst during other periods waters are only
367 weakly stratified, including the quasi-inertial variations between days 316 and 322. These

368 weakly stratified near-inertial, or near-buoyancy as $N \approx f$, temperature variations may
369 evidence slantwise quasi-gyroscopic near-inertial waves, which can have a large vertical
370 component (LeBlond and Mysak, 1978), as opposed to more common near-horizontal near-
371 inertial waves in strongly stratified waters that are barely noticeable in temperature records.

372 The 18-day average spectrum of the 2-s sampled data poorly resolves sub-mesoscales
373 but shows, near the seafloor, a well-resolved slope of $p = -1.4 \pm 0.025$ between a large range of
374 $0.5 < \omega < 6000$ cpd, across the IGW band and well into the turbulence band (Fig. 2b). No
375 transition to a $-5/3$ -slope is observed before roll-off to noise, but this does not exclude an
376 inertial subrange at higher frequencies hidden under white noise, although shear will be
377 limited so close to the seafloor. The observed $p = -7/5$ -slope is found significantly different
378 from $p = -2$ and $-5/3$ over the indicated frequency range of four orders of magnitude and over
379 the range between $100 < \omega < 10^4$ cpd thereby representing convection turbulence. Over a
380 frequency range of half an order of magnitude the slope-error is about ± 0.1 . Albeit not greatly
381 resolved, the range between $\omega_{\max} < \omega < 10$ cpd falls-off more steeply roughly at $p = -2$ and the
382 range between $10 < \omega < 100$ cpd shows a reduced variance that may partially be characterized
383 by intermittency ($p = -1$; Schuster, 1984), but which is not yet explained. Here, it is observed
384 to bridge between $p = -2$ and super-IGW BO-scaling $p = -7/5$. This would be further
385 observation of a marginally ocean-state to the -1 -scaling in KE-spectra (present Fig. 1 and van
386 Haren et al., 2002) and in the continuum of the band $[f N]$ in open-ocean T-spectra (van
387 Haren and Gostiaux, 2009).

388 About 140 m above the seafloor, a less precise older-type T-sensor demonstrates $p = -$
389 $7/5$ between a reduced range of about $10 < \omega < 1000$ cpd, with a suggestion for $p = -5/3$
390 around 10 cpd. This indicates convection can still dominate over shear extending $O(100)$ m
391 above the seafloor, as has been shown in more detail for certain periods (van Haren, 2023c).

392 Whilst more extended work with longer data sets and more T-sensors is to be done,
393 the extended continuous spectral slope from these high-resolution temperature observations
394 suggests a direct coupling between sub-mesoscale motions, IGW motions, comprising

395 internal gravity and gyroscopic waves, and convection turbulence. The temperature spectra
396 also show consistency with the limited KE-spectra of Fig. 1 from roughly the same area, and
397 both indicate a dominance of non-isotropic, stratified-turbulence convection between sub-
398 mesoscales and largest turbulent overturning scales in extended BO-scaling suggesting cross-
399 spectral coupling. The discrepancy with KE-spectra in laboratory experiments of Pawar and
400 Arakeri (2016) may be due to the difference of settings. In a non-zero-mean flow turbulence
401 convection experiment near the gas-liquid critical point, BO-scaling was observed for both
402 KE and temperature (Ashkenazi and Steinberg, 1999). We recall that our deep-sea conditions
403 are non-zero-mean flow, weak tides, very high bulk Reynolds numbers $O(10^5)$ given the large
404 scales, varying non-zero vertical density stratification, and our example spectra did not clearly
405 resolve KO-scaling.

406 This 18-day T-sensor data set demonstrates dominant deviations from inertial
407 subrange over several orders of magnitude of frequency range. The mesoscale-IGW-
408 turbulence motions transport and locally mix warm waters with cooler surroundings outside a
409 period of buoyancy-driven dense-water formation, which is thought to bring cooler waters
410 downward during short periods of time.

411

412 **5 How robust is the system of ocean circulation and stratification?**

413 Any variation to the nonlinear system of ocean circulation may encounter several
414 complex feedback mechanisms, of which the effects are not yet fully understood for the
415 present-day ocean. Although stable density stratification hampers vertical exchange by
416 turbulent mixing, it does not block it. While stratification supports internal waves and their
417 destabilizing shear, turbulent mixing during particular phase of a wave may decrease or
418 destroy it locally in time and space. However, a subsequent internal wave-phase will restratify
419 the mixed patch, thereby maintaining its own support of stable stratification. Such a feedback
420 system may be at work, for example when the ocean absorbs more heat.

421 Increased sea-surface temperature may lead to increased vertical density
422 stratification, which may lead to less turbulent exchange as vertical overturning is suppressed.

423 However, it will also lead to more internal waves through the extension of their spectral band
424 to higher frequencies, with the potential to increased interaction, non-linearity, and
425 turbulence-generating wave breaking. As particular internal waves can propagate deep into
426 the ocean interior away from their source, they can cause enhanced turbulent mixing
427 elsewhere (e.g., Alford, 2003).

428 Limited observations have thus far not provided evidence for an inverse
429 correspondence between changes in turbulent mixing and changes in temperature across the
430 near-surface photic zone along a longitudinal section of the Northeast Atlantic Ocean (van
431 Haren et al., 2021b). This lack of correspondence suggests a feedback mechanism at work
432 mediating potential physical environment changes so that global warming may not affect
433 vertical turbulent fluxes of heat, and thereby also of, e.g., carbon.

434 One such feedback mechanism may be convection-turbulence induced by internal
435 waves and sub-mesoscale eddies. Renewed analysis of yearlong moored current meter data
436 from the Irminger Sea, North-Atlantic Ocean, demonstrate a significant $p = -11/5$ spectral
437 slope at sub- and at super-inertial frequencies (Fig. 3). As was outlined in van Haren (2007),
438 the area showed an IGW-band (1), for $N = f$, with dominant sub-inertial shear at small 8-m
439 vertical scales despite the dominant internal tidal KE. The correspondence with the
440 Mediterranean data of Fig. 1 is striking, including the one order of magnitude change in KE
441 between sub- and super-IGW $p = -11/5$ -slopes with similar $p = -1$ bridge albeit uncertain
442 crossing level, and similar heights of near-inertial peak despite the tidal peak in Fig. 3.

443 While few ocean observations have been presented of BO-scaling thus far in
444 comparison with KO-scaling, perhaps also because of the lack of precision of standard
445 oceanographic instrumentation, coupling has not been established between convection and
446 stratified small-scale turbulence with mesoscale motions. Likewise, complicating factors are
447 spectral interruption by internal waves. However, internal wave trapping by mesoscale eddies
448 has been well described (e.g., Kunze, 1985; Voet et al., 2024), and thus provides an obvious
449 coupling between these motions. It is expected that such coupling may lead to strong
450 nonlinearity of the internal waves that leads to turbulent mixing produced by wave breaking.

451 Although such turbulent mixing is smaller than that induced by internal wave breaking above
452 sloping topography, such coupling may be an important factor in downward transport of near-
453 inertial energy that eventually breaks elsewhere, e.g., over topography.

454 As demonstrated using Mediterranean observations, not only convectively unstable
455 cooler and/or saltier waters potentially lead to downward motions from the surface. Also, sub-
456 mesoscale eddies and near-inertial waves can push stratified waters to the deep sea. Such a
457 downward push can be fast to transport materials from surface to 2500-m deep seafloor in a
458 day (van Haren et al., 2006), and which is of the same order of magnitude as attributed to
459 dense-water convection (Schott et al., 1996). It can also be more turbulent compared to shear-
460 induced motions in the stratified ocean-interior, whereby turbulence reaches the seafloor
461 according to few observations from the abyssal Pacific (van Haren, 2020) and alpine
462 freshwater Lake Garda (van Haren and Dijkstra, 2021). Further extended observational
463 evidence is urgently needed, preferably resolving much larger scales.

464 Although the anthropogenic influence on the Earth's climate is without doubt, the
465 impact on ocean circulation is not fully known because we lack sufficient, notably
466 observational, information of the relevant processes that thus cannot be properly modeled yet.
467 Therefore, we should be cautious in making predictions (e.g., Ditlevsen and Ditlevsen, 2023;
468 van Westen et al., 2024) on future ocean circulation based on single parameters like ocean-
469 surface temperature or fresh-water flux that are uncertain proxies. Because no observational
470 (van Haren et al., 2021b), modeling (Little et al., 2020) or paleo-proxy validation (Cisneros et
471 al., 2019) physics evidence exists that sea-surface temperature is a solid estimator of AMOC-
472 strength variations, other properties like vertical density gradients (stratification), and
473 turbulence intensity may be considered. Small-scale physical processes such as, for example,
474 transport by sub-mesoscale eddies and turbulence-generating breaking of internal waves that
475 are not incorporated in these models will alter such parameters, and thereby statistical
476 analyses. This may lead to feedback mechanisms on property gradients such as density
477 stratification so that large-scale ocean circulations like the AMOC may not collapse.

478 Variability of the ocean in space and time is a key to its dynamics, but it is unclear
479 how robust such variations can be, e.g., whether shifting sites for deep dense-water formation
480 (Gou et al., 2024) may be part of the same system. Observational evidence verifying
481 numerical simulations' outcome, not only predictions but also present-day, of ocean-state is
482 needed. Observations are also required to demonstrate variability in relevant physics
483 processes for model-implementation. Besides eddies and coupling with atmosphere (e.g.,
484 Gent, 2018), numerical models of complex nonlinear ocean circulation should contain
485 internal-wave turbulence with appropriate space and time dependency. The importance of
486 internal wave breaking leading to boundary mixing above sloping topography in general
487 ocean circulation models has been acknowledged in various ways (Scott and Marotzke, 2002;
488 Ferrari et al., 2016).

489 As for the ocean circulation in the horizontal plane near its surface with most impact
490 on mankind, wind will remain the main driver. As long as the Earth rotation does not alter
491 direction, wind will maintain its general course (Wunsch, 2004). The atmosphere remains the
492 key player in the global heat transport across mid-latitudes rather than the ocean.
493 Simultaneously, the importance of processes like stratification and turbulent mixing induced
494 by, e.g., internal wave breaking with or without sub-mesoscale coupling cannot be
495 underestimated for life near the ocean-surface as well as in the -deep, because it will come to
496 a halt without such processes.

497

498 *Data availability.* No new data were created or analyzed in this study: replot and re-analysis
499 of data presented in van Haren and Millot (2003), van Haren (2007) and van Haren (2023a).

500

501 *Competing interests.* The author declares that he has no conflict of interest.

502

503 *Acknowledgments.* I thank L. Gerringa for commenting on a previous draft of the manuscript.

504

505 **References**

- 506 Albérola, C., Millot, C., and Font, J.: On the seasonal and mesoscale variabilities of the
507 Northern Current during the PRIMO-0 experiment in the western Mediterranean Sea.
508 *Oceanol. Acta*, 18, 163-192, 1995.
- 509 Aldama-Campino A., Fransner F., Ödalen, M., Groeskamp, S., Yool, A. Döös, K., and
510 Nycander, J.: Meridional ocean carbon transport, *Global Biogeochem. Cy.*, 34
511 e2029GB006336, 2023.
- 512 Alford, M. H.: Redistribution of energy available for ocean mixing by long-range propagation
513 of internal waves, *Nature*, 423, 159-162, 2003.
- 514 Ashkenazi, S., and Steinberg, V.: Spectra and statistics of velocity and temperature
515 fluctuations in turbulent convection, *Phys. Rev. Lett.*, 83, 4760-4763, 1999.
- 516 Bak, P., Tang, C., and Wiesenfeld, K.: Self-organized criticality: An explanation of the 1/f
517 noise, *Phys. Rev. Lett.*, 59, 381-384, 1987.
- 518 Bolgiano, R.: Turbulent spectra in a stably stratified atmosphere, *J. Geophys. Res.*, 64, 2226-
519 2229, 1959.
- 520 Brainerd, K. E., and Gregg, M. C.: Surface mixed and mixing layer depths, *Deep-Sea Res. I*,
521 42, 1521-1543, 1995.
- 522 Celani, A., Mazzino, A., and Vozella, L.: Rayleigh-Taylor turbulence in two dimensions,
523 *Phys. Rev. Lett.*, 96, 134504, 2006.
- 524 Chunchuzov, I. P., Johannessen, O. M., and Marmorino, G.O.: A possible generation
525 mechanism for internal waves near the edge of a submesoscale eddy, *Tellus A*, 73, 1-11,
526 2021.
- 527 Cisneros, M., Cacho, I., Frigola, J., Snchez-Vidal, A., Calafat, A., Pedrosa-Pàmies, R.,
528 Rumín-Caparrós, A., and Canals, M.: Deep-water formation variability in the north-
529 western Mediterranean Sea during the last 2500 yr: A proxy validation with present-day
530 data, *Glob. Planet. Chang.* 177, 56-68, 2019.

531 Crepon, M., Wald, L., and Monget, J. M.: Low-frequency waves in the Ligurian Sea during
532 December 1977, *J. Geophys. Res.*, 87, 595-600, 1982.

533 Ditlevsen, P., and Ditlevsen, S.: Warning of a forthcoming collapse of the Atlantic meridional
534 overturning circulation, *Nat. Comm.* 14, 4254, 2023.

535 Emanuel, K., *Atmospheric Convection* 580 pp., Oxford Univ. Press, New York, 1984.

536 Eriksen, C. C.: Observations of internal wave reflection off sloping bottoms, *J. Geophys.*
537 *Res.*, 87, 525-538, 1982.

538 Ferrari, R., Mashayek, A., McDougall, T. J., Nikurashin, M. and Campin, J.-M.: Turning
539 ocean mixing upside down, *J. Phys. Oceanogr.*, 46, 2229-2261, 2016.

540 Garrett, C.: The Mediterranean Sea as a climate test basin, In: Malanotte-Rizzoli, P., and
541 Robinson, A. R. eds., *Ocean Processes in Climate Dynamics: Global and Mediterranean*
542 *Examples*, Kluwer Academic Publishes, 227-237, 1994.

543 Garrett, C., and Munk, W.: Space-time scales of internal waves, *Geophys. Fluid Dyn.*, 3, 225-
544 264, 1972.

545 Gascard, J.-C.: Vertical motions in a region of deep water formation, *Deep-Sea Res.*, 20,
546 1011-1027, 1973.

547 Gascard, J.-C.: Mediterranean deep water formation, baroclinic eddies and ocean eddies,
548 *Oceanol. Acta*, 1, 315-330, 1978.

549 Gent, P. R.: A commentary on the Atlantic meridional overturning circulation stability on
550 climate models, *Ocean Mod.*, 122, 57-66, 2018.

551 Gerkema, T., Zimmerman, J. T. F., Maas, L. R. M., and van Haren, H.: Geophysical and
552 astrophysical fluid dynamics beyond the traditional approximation, *Rev. Geophys.*, 46,
553 RG2004, doi:10.1029/2006RG000220, 2008.

554 Gou, R., Wang, Y., Xiao, K., and Wu, L.: A plausible emergence of new convection sites in
555 the Arctic Ocean in a warming climate, *Environ. Res. Lett.*, 19, 031001, 2024.

556 Gregg, M. C.: Scaling turbulent dissipation in the thermocline, *J. Geophys. Res.*, 94, 9686-
557 9698, 1989.

558 Hosegood, P., Bonnin, J., and van Haren, H.: Solibore-induced sediment resuspension in the
559 Faeroe-Shetland Channel, *Geophys. Res. Lett.*, 31, L09301, doi:10.1029/2004GL019544,
560 2004.

561 Kolmogorov, A. N.: The local structure of turbulence in incompressible viscous fluid for very
562 large Reynolds numbers, *Dokl. Akad. Nauk SSSR*, 30, 301-305, 1941.

563 Kunze, E.: Near-inertial wave propagation in geostrophic shear, *J. Phys. Oceanogr.*, 15, 544-
564 565, 1985.

565 LeBlond, P. H., and Mysak, L. A.: *Waves in the ocean*, Elsevier, New York, 602 pp., 1978.

566 Lin, J.-T., Turbulence spectra in the buoyancy subrange of thermally stratified shear flows,
567 143 pp., PhD-thesis Colorado State University, Fort Collins, 1969.

568 Liot, O., Seychelles, F., Zonta, F., Chibbaro, S., Coudarchet, T., Gasteuil, Y., Pinton, J.-F.,
569 Salort, J., and Chillà, F.: Simultaneous temperature and velocity Lagrangian
570 measurements in turbulent thermal convection, *J. Fluid Mech.*, 794, 655-675, 2016.

571 Little, C. M., Zhao, M., and Buckley, M. W.: Do surface temperature indices reflect
572 centennial-timescale trends in Atlantic Meridional Overturning Circulation strength?
573 *Geophys. Res. Lett.*, 47, e2020GL090888, 2020.

574 Liu, Z., Gu, S., Zou, S., Zhang, S., Yu, Y., and He, C.: Wind-steered eastern pathway of the
575 Atlantic Meridional Overturning Circulation, *Nat. Geosci.*, 17, 353-360, 2024.

576 Lohse, D., and Xia, K.-Q.: Small-Scale properties of turbulent Rayleigh-Bénard convection,
577 *Annu. Rev. Fluid Mech.*, 42, 335-364, 2010.

578 Marotzke, J., and Scott, J. R.: Convective mixing and the thermohaline circulation, *J. Phys.*
579 *Oceanogr.*, 29, 2962-2970, 1999.

580 Marshall, J., and Schott, F.: Open-ocean convection: observations, theory, and models, *Rev.*
581 *Geophys.*, 37, 1-64, 1999.

582 McDougall, T. J., and Ferrari, R.: Abyssal upwelling and downwelling driven by near-
583 boundary mixing, *J. Phys. Oceanogr.*, 47, 261-283, 2017.

584 Mertens, C., and Schott, F.: Interannual variability of deep-water formation in the
585 Northwestern Mediterranean, *J. Phys. Oceanogr.*, 28, 1410-1424, 1998.

586 Millot, C.: Circulation in the Western Mediterranean Sea, *J. Mar. Sys.*, 20, 423-442, 1999.

587 Munk, W.: Abyssal recipes, *Deep-Sea Res.*, 13, 707-730, 1966.

588 Munk, W., and Wunsch, C.: Abyssal recipes II: Energetics of tidal and wind mixing, *Deep-*
589 *Sea Res. I*, 45, 1977-2010, 1998.

590 Obukhov, A. M.: Structure of the temperature field in a turbulent flow, *Izv. Akad. Nauk*
591 *SSSR, Ser. Geogr. Geofiz.*, 13, 58-69, 1949.

592 Obukhov, A. M.: Effect of buoyancy forces on the structure of temperature field in a turbulent
593 flow, *Dokl. Akad. Nauk SSSR*, 125, 1246-1248, 1959.

594 Pawar, S. S., and Arakeri, J. H.: Kinetic energy and scalar spectra in high Rayleigh number
595 axially homogeneous buoyancy driven turbulence, *Phys. Fluids*, 28, 065103, 2016.

596 Perkins, H.: Observed effect of an eddy on inertial oscillations, *Deep-Sea Res.*, 23, 1037-
597 1042, 1976.

598 Phillips, O. M.: On spectra measured in an undulating layered medium, *J. Phys. Oceanogr.*, 1,
599 1-6, 1971.

600 Polzin, K. L., Toole, J. M., Ledwell, J. R., and Schmitt, R. W.: Spatial variability of turbulent
601 mixing in the abyssal ocean, *Science*, 276, 93-96, 1997.

602 Polzin, K. L., Kunze, E., Toole, J. M., and Schmitt, R. W.: The partition of finescale energy
603 into internal waves and subinertial motions, *J. Phys. Oceanogr.*, 33, 234-248, 2003.

604 Poujade, O.: Rayleigh-Taylor turbulence is nothing like Kolmogorov turbulence in the self-
605 similar regime, *Phys. Rev. Lett.*, 97, 185002, 2006.

606 Reid, R. O.: A special case of Phillips' general theory of sampling statistics for a layered
607 medium, *J. Phys. Oceanogr.*, 1, 61-62, 1971.

608 Rhein, M.: Deep water formation in the western Mediterranean, *J. Geophys. Res.*, 100, 6943-
609 6959, 1995.

610 Saint-Guilly, B.: On the response of the ocean to impulse, *Tellus* 24, 344-349, 1972.

611 Sarkar, S., and Scotti, A.: From topographic internal gravity waves to turbulence, *Ann. Rev.*
612 *Fluid Mech.*, 49, 195-220, 2017.

613 Schott, F., Visbeck, M., Send, U, Fischer, J., and Desaubies, Y.: Observations of deep
614 convection in the Gulf of Lions, Northern Mediterranean, during the winter of 1991/92, *J.*
615 *Phys. Oceanogr.*, 26, 505-524, 1996.

616 Schuster, H. G., *Deterministic Chaos: An Introduction*, Physik-Verlag, Weinheim, 220 pp.,
617 1984.

618 Scott, J. R., and Marotzke, J, 1998: The location of diapycnal mixing and the meridional
619 overturning circulation, *J. Phys. Oceanogr.*, 32, 3578-3595, 2002.

620 Storer, B. A., Buzzicotti, M., Khatri, H., Griffies, S. M., and Aluie, H.: Global energy
621 spectrum of the general oceanic circulation, *Nat. Comm.*, 13, 5314, 2022.

622 Taira, K., Yanagimoto D., and Kitagawa, S.: Deep CTD casts in the challenger deep. Mariana
623 Trench, *J. Oceanogr.*, 61, 447-454, 2005.

624 Testor, P., and Gascard, J.C.: Post-convection spreading phase in the Northwestern
625 Mediterranean Sea, *Deep-Sea Res.*, 53, 869-893, 2006.

626 Thorpe, S. A.: Transitional phenomena and the development of turbulence in stratified fluids:
627 a review, *J. Geophys. Res.*, 92, 5231-5248, 1987.

628 Thorpe, S. A.: *The turbulent ocean*, Cambridge University Press, Cambridge, 439 pp, 2005.

629 van Haren, H.: Inertial and tidal shear variability above Reykjanes Ridge, *Deep-Sea. Res. I*,
630 54, 856-870, 2007.

631 van Haren, H.: Slow persistent mixing in the abyss, *Ocean Dyn.*, 70, 339-352, 2020.

632 van Haren, H.: Convection and intermittency noise in water temperature near a deep
633 Mediterranean seafloor, *Phys. Fluids*, 35, 026604, 2023a.

634 van Haren, H.: Near-inertial wave propagation between stratified and homogeneous layers, *J.*
635 *Oceanogr.*, 79, 367-377, 2023b.

636 van Haren, H.: Direct observations of general geothermal convection in deep Mediterranean
637 waters, *Ocean Dyn.*, 73, 807-825, 2023c.

638 van Haren, H., and Dijkstra, H. A.: Convection under internal waves in an alpine lake, *Env.*
639 *Fluid Mech.*, 21, 305-316, 2021.

640 van Haren, H., and Gostiaux, L.: High-resolution open-ocean temperature spectra, *J.*
641 *Geophys. Res.*, 114, C05005, doi:10.1029/2008JC004967, 2009.

642 van Haren, H., and Gostiaux, L.: Detailed internal wave mixing observed above a deep-ocean
643 slope, *J. Mar. Res.*, 70, 173-197, 2012.

644 van Haren, H. and Millot, C.: Seasonality of internal gravity waves kinetic energy spectra in
645 the Ligurian Basin, *Oceanol. Acta*, 26, 635-644, 2003.

646 van Haren, H., and Millot, C.: Rectilinear and circular inertial motions in the Western
647 Mediterranean Sea, *Deep-Sea Res. I*, 51, 1441-1455, 2004.

648 van Haren, H., Maas, L., and van Aken, H.: On the nature of internal wave spectra near a
649 continental slope, *Geophys. Res. Lett.*, 29(12), 10.1029/2001GL014341, 2002.

650 van Haren, H., Millot, C., and Taupier-Letage, I.: Fast deep sinking in Mediterranean eddies,
651 *Geophys. Res. Lett.*, 33, L04606, doi:10.1029/2005GL025367, 2006.

652 van Haren, H., Ribó, M., and Puig, P.: (Sub-)inertial wave boundary turbulence in the Gulf of
653 Valencia. *J. Geophys. Res.Oceans*, 118, 2067-2073, doi:10.1002/jgrc.20168, 2013.

654 van Haren, H., Uchida, H., and Yanagimoto, D.: Further correcting pressure effects on
655 SBE911 CTD-conductivity data from hadal depths, *J. Oceanogr.*, 77, 137-144, 2021a.

656 van Haren, H., Brussaard, C. P. D., Gerringa, L. J. A., van Manen, M. H., Middag, R., and
657 Groenewegen, R.: Diapycnal mixing near the photic zone of the NE-Atlantic, *Ocean Sci.*,
658 17, 301-318, 2021b.

659 van Haren, H., Voet, G., Alford, M. H., Fernandez-Castro, B., Naveira Garabato, A. C.,
660 Wynne-Cattanach, B. L., Mercier, H., and Messias, M.-J.: Near-slope turbulence in a
661 Rockall canyon, *Deep-Sea Res. I*, 206, 104277, 2024.

662 van Westen, R. M., Kliphuis, M., and Dijkstra, H.A.: Physics-based early warning signal
663 shows that AMOC is on tipping course, *Sci. Adv.*, 10, eadk1189, 2024.

664 Voet, G., et al.: Near-inertial energy variability in a strong mesoscale eddy field in the Iceland
665 Basin, *Oceanogr.*, 37, <https://doi.org/10.5670/oceanog.2024.302>, 2024.

666 Winters, K. B.: Tidally driven mixing and dissipation in the stratified boundary layer above
667 steep submarine topography, *Geophys. Res. Lett.*, 42, 7123-7130, 2015.

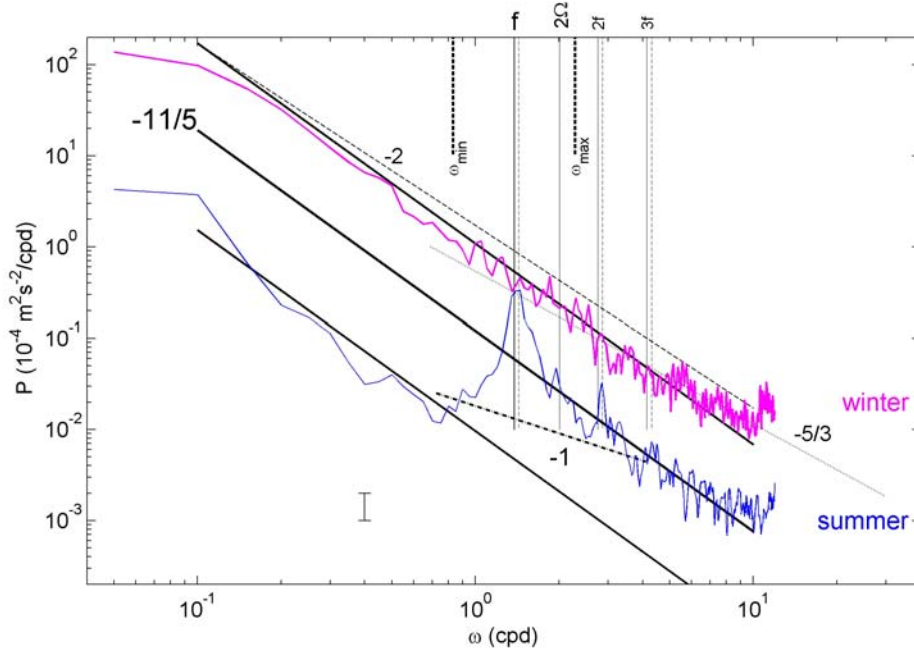
668 Wunsch, C.: Gulf Stream safe if wind blows and Earth turns, *Nature*, 428, 601, 2004.

669 Wunsch, C., and Ferrari, R.: Vertical mixing, energy and the general circulation of the oceans,
670 *Ann. Rev. Fluid Mech.*, 36, 281-314, 2004.

671 Wynne-Cattanach, B. L., Couto, N., Drake, H. F., Ferrari, R., Le Boyer, A., Mercier, H.,
672 Messias, M.-J., Ruan, X., Spingys, C. P., van Haren, H., Voet, G., Polzin, K., Naveira
673 Garabato, A., and Alford, M. H.: Observational evidence of diapycnal upwelling within a
674 sloping submarine canyon, *Nature*, 630, 884-890, 2024.

675 Xu, Y., and Fu, L.-L.: The effects of altimeter instrument noise on the estimation of the
676 wavenumber spectrum of sea surface height, *J. Phys. Oceanogr.*, 42, 2229-2233, 2012.

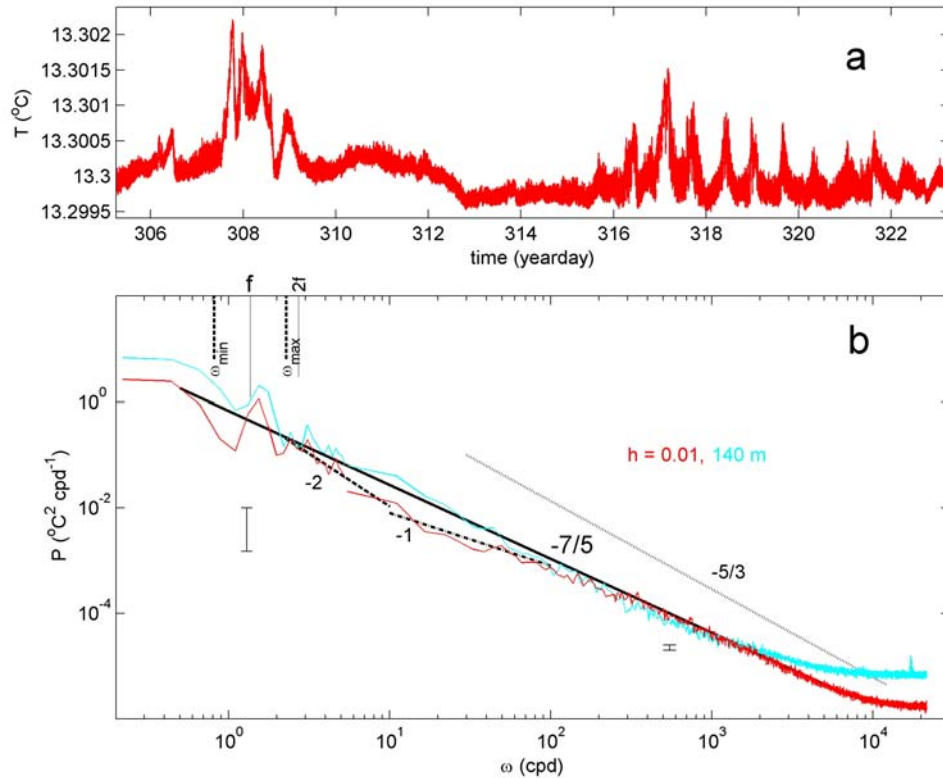
677



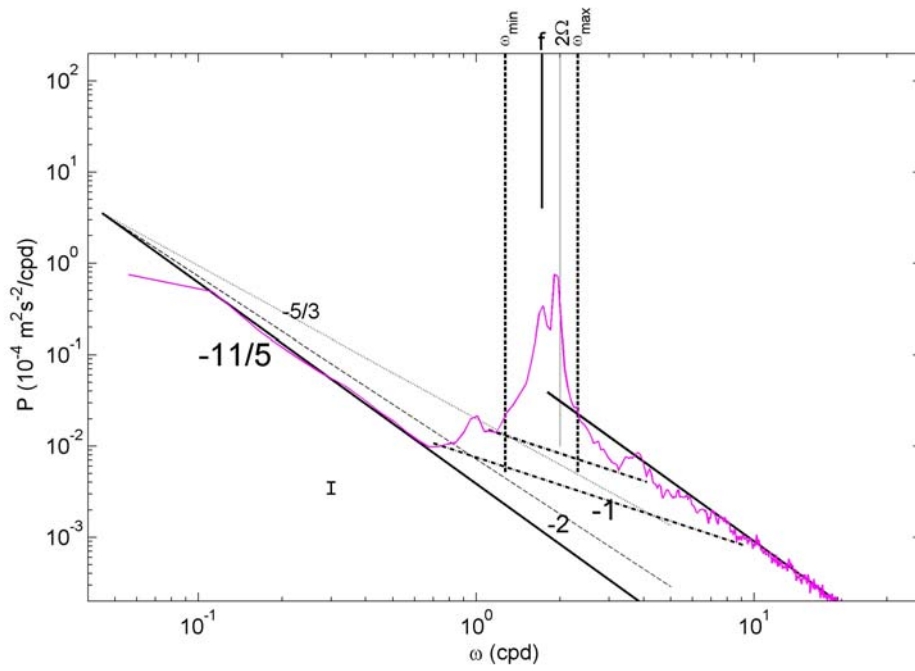
679

680 **Fig. 1.** Moderately smoothed (20 degrees of freedom, dof) kinetic energy (KE) spectra over
 681 100 days of data from 3600-s sampled Aanderaa mechanical current meter moored in
 682 1981/1982 at $z = -1100$ m well above the continental slope in the Ligurian Sea at $43^\circ 28.32'$
 683 N, $7^\circ 46.10'$ E, 2250 m water depth. For details on these data, see van Haren and Millot
 684 (2003). The two spectra are not offset deliberately from each other; ‘noise’ also contains other
 685 signals near the Nyquist frequency. The ‘summer’ spectrum (blue) is an average from data
 686 between days 190 and 290 (in 1981), the ‘winter’ (magenta) between days 375 and 475
 687 (adding +365 for days in 1982). Several frequencies are indicated including inertial frequency
 688 f , Earth rotational Ω and inertio-gravity wave bounds [$\omega_{\min} \leq f$, $\omega_{\max} \geq N, 2\Omega$] for buoyancy
 689 frequency $N = f$. The dashed lines indicate harmonics of $1.04f$. Four spectral slopes ω^p are
 690 indicated by their exponent: $p = -11/5$ (solid slope in the log-log plot) for Bolgiano-Obukhov
 691 ‘BO’ scaling reflecting the buoyancy subrange of convection-turbulence (e.g., Pawar and
 692 Arakeri, 2016), $p = -5/3$ (dotted slope) for Kolmogorov-Obukhov ‘KO’ scaling reflecting the
 693 equilibrium inertial subrange for dominant shear-induced turbulence (Kolmogorov 1941;
 694 Obukhov, 1949), $p = -1$ (dash-dotted slope) for intermittency of self-organized criticality
 695 (Schuster, 1984; Bak et al., 1987) and $p = -2$ (dashed slope) for internal wave scaling (Garrett
 696 and Munk, 1972) or finestructure contamination (Phillips, 1971; Reid, 1971).

697



698
 699 **Fig. 2.** Eighteen days of high-resolution 2-s sampled temperature ‘T’ data from a NIOZ
 700 T-sensor fallen off a mooring-line in 2020 and lying 0.01 m above a flat seafloor about 10
 701 km south of the foot of the continental slope at 42° 49.50’ N, 6° 11.78’ E, 2458 m water
 702 depth, about 100 km WSW from the site in Fig. 1. For details on these data see van Haren
 703 (2023a). (a) Time series of 18 days of raw temperature data. (b) Temperature variance
 704 spectrum that is stitched together using two spectra with different smoothing. Weakly
 705 smoothed (10 dof; $\omega < 5$ cpd) and heavily smoothed (250 dof; $\omega > 5$ cpd) spectra of data in
 706 a., with bars showing the respective 95% confidence limits. For comparison, a spectrum
 707 is shown in cyan from data of a less precise T-sensor at a drag-parachute line stuck at 140
 708 m above the seafloor. Frequency and spectral slope indications are as in Fig. 1, while -7/5
 709 (solid slope) indicates BO-scaling of an active scalar (e.g., Pawar and Arakeri, 2016).
 710 Note the different axes-ranges compared with Fig. 1.



711
 712 **Fig. 3.** Like Fig. 1 with the same axes ranges, but for strongly smoothed (50 dof) KE
 713 spectra averaged over 400 days of data from 600-s sampled Valeport mechanical current
 714 meter moored at $z = -1000$ m over the Mid-Atlantic Ridge at $58^\circ 59.67' \text{ N}$, $33^\circ 56.12' \text{ W}$,
 715 2540 m water depth in 2003/2004, within the project discussed in van Haren (2007). The
 716 small bar shows the 95% confidence interval.
 717